Influence of the spatial, temporal, and concentrational dependence of the diffusion coefficient on dopant dynamics: optimization of annealing time

E. L. Pankratov*
Institute for Physics of Microstructures of RAS, 603950, Nizhny Novgorod, GSP-105, Russia
(Received 24 November 2004; revised manuscript received 16 May 2005; published 1 August 2005)

It has recently been shown that the interface between layers of a heterostructure makes it possible to increase the sharpness of the *p-n* junction and the homogeneity of an impurity distribution in doped areas, and also to control the depth of the junction. In this work the dynamics of a dopant concentration in an inhomogeneous semiconductor structure has been analyzed, taking into account the temporal and concentrational dependence of the diffusion coefficient. The optimization of the parameters and the annealing time for production of the *p-n* junction with smaller parasitic capacitance has been done. It has been shown that doubling the annealing time in comparison with its optimal value leads to variation of the sharpness of the *p-n* junction from 10% to 200%.

DOI: 10.1103/PhysRevB.72.075201 PACS number(s): 72.20.−i, 85.40.Ry, 73.40.Lq, 66.30.−h

I. INTRODUCTION

The increase of performance and reliability of microelectronic devices is attracting great interest. One way to achieve this goal is to decrease the parasitic capacitance of a *p-n* junction by increasing its sharpness.[1–3] On the other hand, the increase of homogeneity of impurity distribution in doped areas of a semiconductor structure allows it to operate with higher current densities and to decrease local overheats, thus increasing the performance of semiconductor devices.[1,2,4]

For production of *p-n* junctions different types of technological processes, such as diffusion at high temperatures and ion implantation in homogenous samples,[1–6] are used. At the present time, with dimensions of semiconductor devices decreasing, a dopant diffusion has major interest. Let us consider in this paper an epitaxial layer with the thickness a $(0\leqslant x\leqslant a)$ and the diffusion coefficient D_1, which has been sputtered on a substrate with the thickness $L-a$ $(a\leqslant x\leqslant L)$, with the diffusion coefficient $D_2<D_1$, and with known type of conductivity (p or n) (see Fig. 1). Here L is the full length of the heterostructure. Let us consider a dopant, which was infused across the boundary $x=0$ into the heterostructure for production of the second type of conductivity (n or p) in the epitaxial layer. At the time $t=0$ the temperature of the heterostructure has been increased. This heating leads to diffusion of the infused dopant into the heterostructure during the time t_a. After the time interval t_a, the heterostructure has been cooled and the dopant diffusion stopped. Such technological processes are used, for example, in semiconductor-on-insulator technology.[7]

The aim of the present paper is to investigate the influence of spatial, temporal, and concentrational dependence of the diffusion coefficient of a heterostructure on the technological process and to optimize the annealing time t_a to increase the sharpness of the *p-n* junction and to increase the homogeneity of impurity concentration in doped areas.

II. METHOD OF SOLUTION

For optimization of production of *p-n* junctions the dopant dynamics have been analyzed. Spatiotemporal distribution of dopant concentration in the considered heterostructure (see Fig. 1) is described by the second Fick's law

$$\frac{\partial C(x,t)}{\partial t}=-\frac{\partial J(x,t)}{\partial x}, \tag{1}$$

where $J(x,t)=-D[\partial C(x,t)/\partial x]$ is a dopant flow. The diffusion coefficient of semiconductor D depends on temperature (see, for example, Refs. 4 and 8). Therefore, if the temperature of the semiconductor varies in space and/or time, then the diffusion coefficient also varies in space and/or time: $D=D(x,t)$. The diffusion coefficient of an inhomogeneous semiconductor, such as a heterostructure, also depends on coordinate $D=D(x)$. High doping of semiconductor materials leads to increased interaction between dopant atoms and point defects. The interaction corresponds to concentrational dependence of the diffusion coefficient $D=D(C(x,t))$.

The diffusion equation is complemented by boundary and initial conditions. The conditions depend on the type of dop-

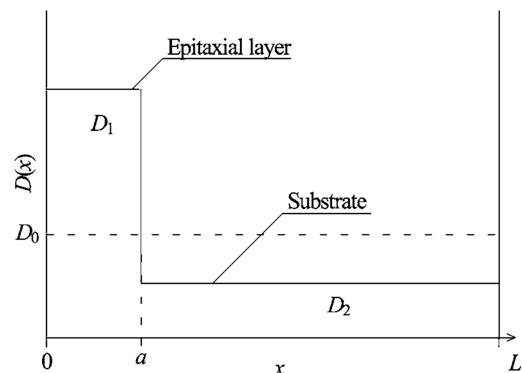

FIG. 1. Step-function spatial distribution of the diffusion coefficient in the heterostructure.

 ©2005 The American Physical Society

ant source. If the quantity of infused dopant is small, then the dopant source is named as finite. For this type of source the boundary and initial conditions for Eq. (1) are

$$J(0,t) = J(L,t) = 0, \quad C(x,0) = f(x). \tag{2}$$

In this case let us introduce the following normalization of a dopant quantity $M=\int_0^L C(x,t)dx=1$ for simplification of the analysis of dopant dynamics. Infusing of a small quantity of dopant is necessary when the first or the third type of dopant will be infused in the doping structure after or during infusing of the second type of dopant (for production of structures with some *p-n* junctions, such as transistor structures). The quantity of the new type of infused dopant must be essentially larger than the quantity of the previous one.

If the quantity of the infused dopant is large, then the dopant source is named as an infinite and the boundary and initial conditions for Eq. (1) can be written in the form

$$C(0,t) = N_1, \quad J(L,t) = 0, \quad C(x > 0,0) = 0. \tag{3}$$

One can assume that the dopant is infused in the heterostructure from an infinite source with the boundary layer concentration N_1. This concentration is essentially larger than the limit of solubility of impurity N_2 in the structure considered in Fig. 1 ($N_1 \gg N_2$). This type of dopant source is used for infusing of the latter type of dopant for maximal difference between their quantities. In the case of an infinite source of dopant the quantity of the dopant depends on time $M=M(t)$.

It has been shown in Ref. 4 that in high-doped materials, interaction between dopant atoms and point defects increases. If the point defects have nonzero charge γe with e an elementary charge, then the interaction leads to concentrational dependence of the diffusion coefficient. The dependence can be approximated by a power law: $D(x,t,C(x,t))=D(x,t)\{1+\mu[C(x,t)/N_2]^\gamma\}$, where $0 \leqslant \mu \leqslant 1$. Usually the parameter γ is an integer in the interval $1 \leqslant \gamma \leqslant 3$ (see Refs. 4, 9, and 10). If the dopant source is finite, one can neglect the concentrational dependence of the diffusion coefficient and consider the case $\mu=0$. Let us determine the solution of the diffusion equation (1) and use it for analysis of dopant dynamics. To obtain an analytical solution of Eq. (1) let us use the previously elaborated approach[11,12] and transform the spatial, temporal, and concentrational dependence of the diffusion coefficient as: $D(x,t,C(x,t))=D_0[1+\epsilon h(x,t)]\{1+\mu[C(x,t)/N_2]^\gamma\}$, where $0 \leqslant \epsilon < 1$, $|h(x,t)| \leqslant 1$, and D_0 is the average value of the diffusion coefficient. We look for an analytical solution of Eq. (1) in the power series form

$$C(x,t) = \sum_{k=0}^{\infty} \epsilon^k \sum_{m=0}^{\infty} \mu^m C_{km}(x,t). \tag{4}$$

By substitution of (4) into (1) and equating the coefficients with the same power of ϵ and μ, one can obtain the system of equations for the functions $C_{km}(x,t)$. Substitution of the decomposition (4) into the boundary and initial conditions (2) and (3) gives the analogous conditions for the system of equations for the functions $C_{km}(x,t)$.

This approach allows us to determine an analytical solution of the diffusion equation in the case of spatial, temporal, and concentrational dependence of the diffusion coefficient for the case of small values of parameters ϵ and μ. In other papers (see, for example, Refs. 4, 9, and 13) an analytical solution of Eq. (1) was determined only for a few model dependences of the diffusion coefficient on one parameter: on coordinate $D(x)$, on time $D(t)$, or on concentration $D(C(x,t))$, or even for the asymptotical case of constant diffusion coefficient D_0. The analytical approach leads to a faster understanding of the physics in comparison with the numerical one, but computer simulations can be used for any values of ϵ and μ and allows us to obtain the results with high accuracy. Therefore, in this paper both approaches (analytical and numerical) have been used. To solve the diffusion Eq. (1) numerically, we use the standard explicit difference scheme.

The zero-order approximation of dopant concentration for a finite [Eq. (5)] and an infinite [Eq. (6)] source can be written as

$$C_{00}(x,t) = \frac{1}{L} + \frac{2}{L}\sum_{n=1}^{\infty} \int_0^L f(v)\cos\left(\frac{\pi n y}{L}\right)dy \times \cos\left(\frac{\pi n x}{L}\right)\exp\left(-\frac{\pi^2 n^2 D_0 t}{L^2}\right). \tag{5}$$

$$C_{00}(x,t) = N_2\left\{1 - \frac{2}{\pi}\sum_{n=0}^{\infty} \sin\left[\frac{\pi(n+0.5)x}{L}\right] \times \frac{1}{n+0.5}\exp\left[-\frac{\pi^2(n+0.5)^2 D_0 t}{L^2}\right]\right\}. \tag{6}$$

The first- and second-order corrections of dopant concentration take the forms for a finite source of dopant

$$C_{10}(x,t) = \frac{D_1}{L}\sum_{n=1}^{\infty} c_n(x,t)\sum_{m=1}^{\infty}\int_0^t \tilde{e}_{mn}(u) \times mF_m[G_{n+m}(u) - G_{n-m}(u)]du,$$

$$C_{20}(x,t) = \frac{D_1^2}{L}\sum_{n=1}^{\infty} c_n(x,t)\sum_{k=1}^{\infty} k^2 \sum_{m=1}^{\infty} mF_m \times \int_0^t \tilde{e}_{kn}(u)[G_{n-k}(u) - G_{n+k}(u)] \times \int_0^u \tilde{e}_{mk}(\tau)[G_{k-m}(\tau) - G_{k+m}(\tau)]d\tau du, \tag{7}$$

where $F_m=\int_0^L f(v)\cos(v_m y)dy$, $v_n=\pi n/L$, $c_n(x,t)=n\cos(v_n x)e_n(t)$, $s_n(x)=n\sin(v_n x)e_n(t)$, $e_n(t)=\exp[-v_n^2 D_0 t]$, $G_n(t)=\int_0^L \eta(y,t)\cos(v_n y)dy$, $D_1=2D_0\pi^2 L^{-3}$, $\tilde{e}_{mn}(t)=e_{m+0.5}(t)e_{n+0.5}(-t)$. The solutions for C_{10}, C_{20}, C_{01}, C_{02}, C_{11} for an infinite source of dopant have a rather complicated form and are presented in the Appendix.

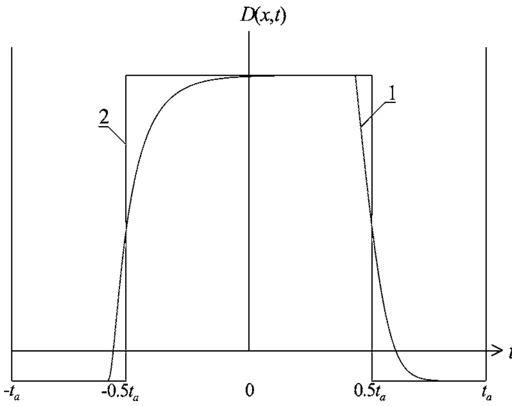

FIG. 2. Temporal dependence of the diffusion coefficient (curve 1) and its approximation (curve 2) by the sum of the average value of the diffusion coefficient and the Walsh function of the second order.

III. DISCUSSION

Let us consider only the second-order approximation of dopant concentration on parameters ϵ and μ, i.e., $C(x,t) \approx C_{00}(x,t) + \epsilon C_{10}(x,t) + \epsilon^2 C_{20}(x,t) + \mu C_{01}(x,t) + \mu^2 C_{02}(x,t) + \epsilon\mu C_{11}(x,t)$. This approximation allows us to analyze dopant dynamics without bulky calculations and to give recommendations for increasing the steepness of impurity distribution in p-n junctions and increasing the homogeneity of impurity distribution in the enriched areas.

Let us analyze some dependences of spatial distribution of impurity concentration on different parameters. Usually the annealing time t_a is larger than the heating and cooling times (t_h and t_c, respectively). The annealing process leads to production of p-n junctions with higher sharpness of impurity profile, when $t_a \gg t_h$ and $t_a \gg t_c$.[11,14] Therefore, let us approximate the temporal dependence of the diffusion coefficient by the sum of the average value of the diffusion coefficient and the Walsh function of the second order (the approximation has been described in Ref. 14 and is illustrated in Fig. 2).

Further let us consider the influence of the variation of parameters ϵ and μ on dopant dynamics. Spatial distribution of impurity concentration is presented in Figs. 3 and 4 for different values of parameter ϵ. As is seen in these figures, increasing the semi-insulating property of the interface between the layers of heterostructure (i.e. increasing the difference between diffusion coefficients in the layers; see Figs. 3 and 4) and the values of parameters μ and γ allows us to increase the steepness of the impurity profile in the substrate. Increasing the steepness of the impurity profile corresponds to a decrease of the parasitic capacity of the p-n junction. It should be noted that the limit of small ϵ have a technological relevance. For example, widely used dopants As and B are infused in an Si/Ge heterostructure at $\epsilon \sim 0.075$ and $\epsilon \sim 0.09$, respectively, for the annealing temperature $T \sim 1000$ K.

For quantitative estimation of the enriched area of a heterostructure let us introduce the effective thickness of the area $\ell(t)$. Two criteria can be used for estimation of the thickness of enriched area. The first one is the estimation of the thickness as the length of decreasing of impurity concentration at 3 dB. The second criterion, which allows us to obtain an analytical approximation of the thickness $\ell(t)$, is the rectangle with the equal square

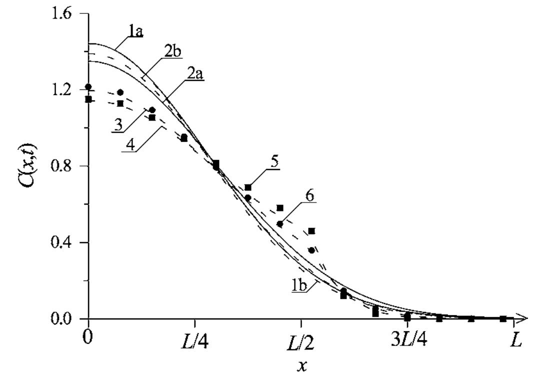

FIG. 3. Spatial distribution of an impurity concentration for the time $t_a = 0.05L^2/D_0$ for the finite source with initial distribution $C(x,0) = \delta(x)$ for different values of parameter ϵ. Solid curves are analytical solutions of diffusion equation (1). Dashed curves are numerical solutions of diffusion equation (1) with conditions (2). Curves 1 correspond to a homogeneous structure ($\epsilon = 0$); curves 2 correspond to $\epsilon = 0.1$; curve 3 corresponds to $\epsilon = 0.62$; and curve 4 corresponds to $\epsilon = 0.84$. Curves 5 and 6 correspond to experimental data for $\epsilon = 0.62$ (Ref. 15) (circles) and $\epsilon = 0.84$ (Ref. 7) (rectangles), respectively.

$$\ell(t) = \frac{1}{C(0,t)} \int_0^L C(x,t)dx. \qquad (8)$$

The last criterion is the optimal one[17] that is widely used for the estimation of different temporal characteristics.[11,12,18–20] Both criteria give us approximately the same results.

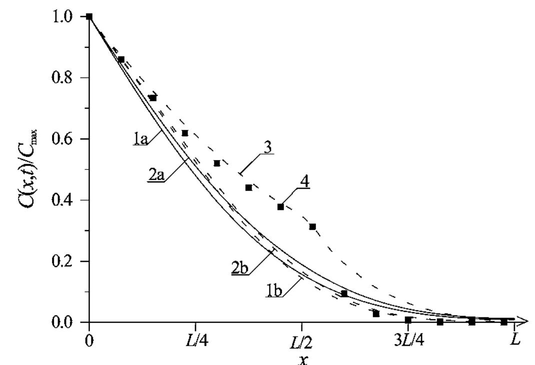

FIG. 4. Spatial distribution of an impurity concentration for the time $t_a = 0.075L^2/D_0$ for an infinite source for different values of parameter ϵ. Solid curves are analytical solutions of diffusion equation (1). Dashed curves are numerical solutions of diffusion equation (1) with conditions (2). Curves 1 correspond to homogeneous structure ($\epsilon = 0$); curves 2 correspond to $\epsilon = 0.1$; the curve 3 corresponds to $\epsilon = 0.78$. The curve 4 (rectangles) corresponds to experimental data for $\epsilon = 0.78$ (Ref. 16).

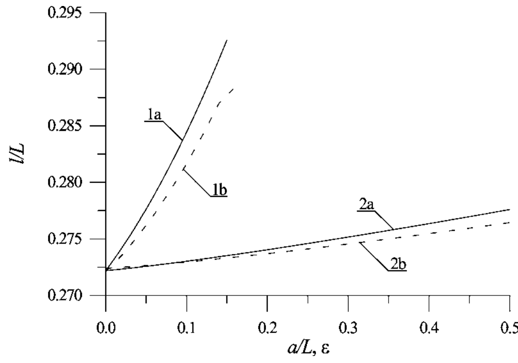

FIG. 5. Dependences of the effective thickness of an impurity distribution for the time $t_a=0.05L^2/D_0$ and the finite source on: parameter ϵ for $a=L/2$ (curves 1), and relation a/L for $\epsilon=0.1$ (curves 2). Solid lines are analytical results. Dashed lines are numerical results.

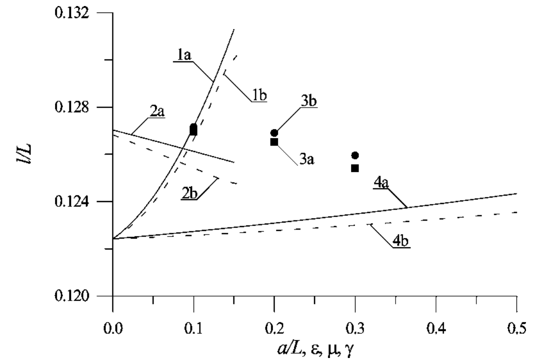

FIG. 6. Dependences of the effective thickness of an impurity distribution for the time $t_a=0.075L^2/D_0$ and an infinite source on: parameter ϵ for $a=L/2$, $\mu=0.1$, and $\gamma=1$ (curve 1); parameter μ for $a=L/2$, $\epsilon=0.1$, and $\gamma=1$ (curve 2); parameter $\gamma/10$ for $a=L/2$ and $\epsilon=\mu=0.1$ (curve 3); and parameter a/L for $\epsilon=\mu=0.1$ and $\gamma=1$ (curve 4). Solid lines and line 3*a* are analytical results. Dashed lines and line 3*b* are numerical results.

Let us consider in this paper the only example of the thickness of enriched area for the fixed annealing time, because the general result is very bulky. Consideration of one example is enough for illustration of major physical effects, which are correlated with dependences of the thickness $\ell(t)$ on different parameters. By analytical calculation of the integrals in (5)–(8) and (A1)–(A5) and numerical summation of the sums in derived formulas for different values of ϵ and a/L, one can approximate the obtained results by the following function for the finite source of dopant with the initial distribution $f(x)=\delta(x)$:

$$\ell(t=0.05L^2/D_0) = [0.396+0.775(a/L)^{1.322}\epsilon-0.6(a/L)^{0.585}\epsilon^2]L.$$

For an infinite source of dopant the same approximation of the function $\ell(t)$ may be obtained in the following form:

$$\ell(t=0.075L^2/D_0) = [0.339+0.22(a/L)^{0.043}\epsilon+1.06(a/L)^2\epsilon^2+\psi]L,$$

where

$$\psi=\begin{cases}0.6(a/L)^{2.9}\epsilon\mu-0.0169\mu-0.002\mu^2, & \gamma=1\\ 0.54(a/L)^{0.678}\epsilon\mu-0.036\mu-0.003\mu^2, & \gamma=2\\ 0.08(a/L)^{0.332}\epsilon\mu-0.006\mu-0.004\mu^2, & \gamma=3.\end{cases}$$

Some dependences of the last approximations are presented in Figs. 5 and 6. The dependences illustrate that increasing the parameter ϵ and ratio a/L and decreasing μ and γ leads to the increase of the area with approximately homogenous impurity distribution (i.e., enriched area).

The spatial distribution of impurity concentration depends on the annealing time: increasing of the annealing time leads to the increase of homogeneity of impurity distribution in the heterostructure. However, the impurity profile, which has the main practical interest, must be almost constant in the area $0\leqslant x\sim a$, but must rapidly decrease in the other region. So, it is necessary to determine an annealing time that corresponds to a compromise between homogeneity of impurity in the epitaxial layer and rapid decrease of impurity concentration in the substrate. For estimation of the compromise annealing time one can use two criteria. Both criteria give us approximately equal results. Let us introduce the function $\beta(x,t)=C(x,t)/C(0,t)$, which characterizes the decrease of impurity concentration with the increase of coordinate. The interface between layers of heterostructure simplifies the production of the distribution with higher homogeneity of impurity in the epitaxial layer and rapid decrease of impurity concentration in the substrate. So, one can define the compromise annealing time from the following condition: $\beta(a,t_a)=1/\sqrt{2}$. This condition corresponds to the decrease of impurity concentration at 3 dB in the epitaxial layer in such a distribution, which was formed during the compromise annealing time. The second way to estimate the compromise annealing time is to approximate the real spatial distribution of impurity concentration by the stepwise function and to minimize the following mean-squared error:

$$U(l_f,t)=\int_0^L\{C(x,t_a)-C_f[1(x)-1(x-l_f)]\}^2dx,$$

where $1(x)$ is the unit step function. As a result of calculation of the annealing time at compromise, the following second-order approximations are obtained: for the finite source of dopant with the initial distribution $f(x)=\delta(x)$

$$t_{ac}\approx[0.36-0.2(a/L)^{1/3}\epsilon+5.814(a/L)^{1.17}\epsilon^2]a^2/D_0,$$

for an infinite source of dopant

$$t_{ac}=[0.912(a/L)^{-0.02}-2.14(a/L)^{-0.5}\epsilon+63.75(a/L)^{-0.93}\epsilon^2 + \xi]a^2/D_0,$$

where

$$\xi = \begin{cases} 2.295(a/L)^{3.17}\mu - 0.6(a/L)^{0.263}\mu^2 - 3.025(a/L)^{3.367}\epsilon\mu, & \gamma = 1 \\ 2.2(a/L)^{3.115}\mu - 4.44(a/L)^{1.7}\mu^2 - 2.048(a/L)^{1.807}\epsilon\mu, & \gamma = 2 \\ 1.238(a/L)^{2.46}\mu - 6.6(a/L)^{2.89}\mu^2 - 1.04(a/L)^{1.678}\epsilon\mu, & \gamma = 3. \end{cases}$$

The obtained approximations are illustrated in Figs. 7 and 8. It follows from the figures that the compromise annealing time increases with the reduction of μ, γ, and the ratio a/L and decreases with the reduction of ϵ.

We note that the annealing time for $\epsilon=0$ is approximately equal to double the annealing time for $\epsilon=1$ $[\tau_a(\epsilon=0) = 2.16\tau_a(\epsilon=1)$ for the finite source of dopant and $\tau_a(\epsilon=0) = 1.82\tau_a(\epsilon=1)$ for an infinite one]. The annealing time for $\epsilon = 1$ is equal to the relaxation time τ_{rel} of dopant concentration in the epitaxial layer. The relaxation time is equal to $\tau_{rel} = a^2/6D_0$ for the finite source of dopant[11,17] and $\tau_{rel} = a^2/2D_0$ for an infinite source of dopant.[12]

IV. LIMITS OF APPLICABILITY

The limits of applicability of analytical description can be determined by numerical calculation of dopant concentration and/or by analytical calculation of corrections to concentration of the third, the fourth, etc. orders. As is seen in Figs. 5–8 the second-order approximation of dopant concentration is applicable when ϵ and μ are not larger than $\epsilon \sim 0.15$ and $\mu \sim 0.2$. For $\epsilon \leq 0.15$ and $\mu \leq 0.2$ the error does not exceed 10%.

V. CONCLUSION

In the present paper the analysis of dopant dynamics in a semiconductor structure, accounting for spatial, temporal, and concentrational dependence of diffusion coefficient, has been done. Certain conditions on these dependences for obtaining the compromise between increasing of homogeneity of impurity distribution in the doped area of the heterostructure and increasing of sharpness of *p*-*n*-junction are obtained. The annealing time has been optimized to achieve the same compromise. The effective thickness of the doped area of the heterostructure was calculated. It has been shown that the increasing of the difference between diffusion coefficients D_1 and D_2 leads to an increase of the effective thickness and to a decrease of the annealing time. The increase of the ratio of thicknesses of the heterostructure layers $a/(L-a)$ leads to an increase of the thickness of the enriched area and to an increase of the optimal annealing time. If the annealing time is approximately equal to its optimal value, the impurity profile and the thickness $\ell(t)$ weakly depend on time. However, doubling the annealing time in comparison with its optimal value leads to variation of the effective thickness $\ell(t)$ and the sharpness $\beta(x,t)$ of the *p*-*n* junction from 25% to 80% and from 10% to 200%, respectively. Thus, fine-tuning the parameters of the technological process and semiconductor structure allows us to significantly improve the properties of *p*-*n* junctions.

ACKNOWLEDGMENTS

This work has been supported by a grant from the Scientific Schools of Russia (Project No. SS-1729.2003.2) and by Russian Foundation of Basic Research (Project No. 05-02-17340-a).

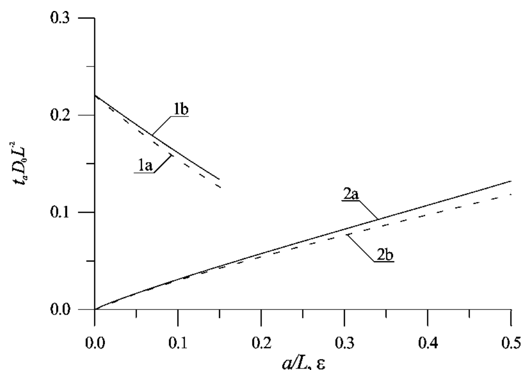

FIG. 7. Dependences of the compromise annealing time for the finite source, on: parameter ϵ for $a=L/2$ (curve 1), and relation a/L for $\epsilon=0.1$ (curve 2). Solid lines are analytical results. Dashed lines are numerical results.

APPENDIX

The corrections of a dopant concentration of the first and the second order for the case of an infinite source are presented in the Appendix. First-order corrections are

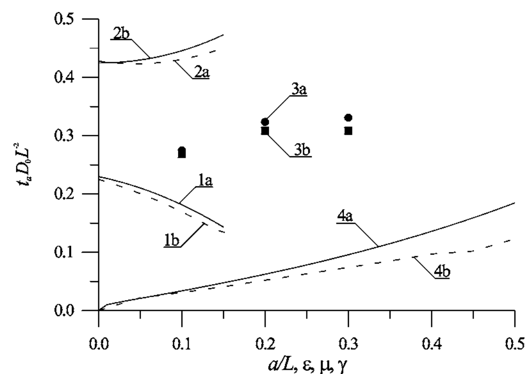

FIG. 8. Dependences of the compromise annealing time for an infinite source on: parameter ϵ for $a=L/2$, $\mu=0.1$, and $\gamma=1$ (curve 1); parameter μ for $a=L/2$, $\epsilon=0.1$, and $\gamma=1$ (curve 2); parameter $\gamma/10$ for $a=L/2$ and $\epsilon=\mu=0.1$ (curve 3); and parameter a/L for $\epsilon=\mu=0.1$ and $\gamma=1$ (curve 4). Solid lines and line $3a$ are analytical results. Dashed lines and line $3b$ are numerical results.

$$C_{10}(x,t)=\frac{D_1N_2}{\pi}\sum_{n=0}^{\infty}s_{n+0.5}(x,t)\times\sum_{m=0}^{\infty}\int_0^t\widetilde{e}_{mn}(u)[H_{n-m}(u)+H_{n+m+1}(u)]du, \quad (A1)$$

where $H_n(t)=\int_0^L\eta(y,t)\sin(v_ny)dy$, $s_n(x)=n\sin(v_nx)e_n(t)$,

$$C_{01}(x,t)=\alpha_2-\gamma\alpha_1, \quad (A2)$$

where

$$\alpha_1=\frac{2N_2}{\pi^3}\sum_{n=0}^{\infty}(n+0.5)s_{n+0.5}(x,t)\times\sum_{k=0}^{\infty}\frac{1}{k+0.5}\sum_{n=0}^{\infty}[e_{km}(t)-e_{n+0.5}(t)][(n+0.5)^2-(m+0.5)^2-(k+0.5)^2][(m+0.5)^2-(n-k)^2]^{-1}-[(m+0.5)^2-(n+k+1)^2]^{-1}\},\quad e_{km}(t)=e_{k+0.5}(t)e_{m+0.5}(t),$$

$$\alpha_2=0 \text{ for } \gamma<3,$$

and

$$\alpha_2=\frac{N_2}{\pi^5}\sum_{n=0}^{\infty}s_n(x,t)\sum_{k=0}^{\infty}\frac{1}{k+0.5}\sum_{l=0}^{\infty}\frac{1}{l+0.5}\times\sum_{i=0}^{\infty}\frac{1}{i+0.5}\sum_{j=0}^{\infty}\frac{e_{klij}(t)-e_{n+0.5}(t)}{j+0.5}[(n+0.5)^2-(k+0.5)^2-(l+0.5)^2-(i+0.5)^2-(j+0.5)^2)\{[(n+0.5)^2-(k-l+i-j)^2]^{-1}-[(n+0.5)^2-(k-l-i+j)^2]^{-1}-[(n+0.5)^2-(k-l+i+j+1)^2]^{-1}-[(n+0.5)^2-(k-l-i-j+1)^2]^{-1}-[(n+0.5)^2-(k+l+i-j+1)^2]^{-1}-[(n+0.5)^2-(i-j-k-l+1)^2]^{-1}+[(n+0.5)^2-(i+j-k-l)^2]^{-1}+[(n+0.5)^2-(i+j+k+l+2)^2]^{-1}\} \text{ for } \gamma=3.$$

Second-order corrections of a dopant concentration are

$$C_{20}(x,t)=-\frac{D_1^2N_2}{2\pi}\sum_{k=1}^{\infty}s_{k+0.5}(x,t)\sum_{n=1}^{\infty}(n+0.5)^2\times\sum_{m=1}^{\infty}\int_0^t\widetilde{e}_{nk}(u)[H_{n+k+1}(u)+H_{n-k}(u)]\times\int_0^u\widetilde{e}_{mn}(\tau)[H_{n+m+1}(\tau)+H_{n-m}(\tau)]d\tau du, \quad (A3)$$

$$C_{02}(x,t)=\gamma^2\alpha_3-\alpha_4, \quad (A4)$$

where

$$\alpha_3=\frac{4N_2}{\pi^5}\sum_{n=0}^{\infty}(n+0.5)^3s_{n+0.5}(x)e_{n+0.5}(t)\times\sum_{k=0}^{\infty}\frac{1}{k+0.5}\sum_{l=0}^{\infty}(l+0.5)^3\sum_{m=0}^{\infty}\frac{n+0.5}{(l+0.5)^2-(n-k)^2}\times\frac{k+0.5}{(l+0.5)^2-(n+k+1)^2}\sum_{i=0}^{\infty}\frac{1}{i+0.5}\sum_{j=0}^{\infty}(l+0.5)\times\frac{[(n+0.5)^2-(l+i+1)^2]^{-1}[(j+0.5)^2-(l-i)^2]^{-1}}{(l+0.5)^2-(i+0.5)^2-(j+0.5)^2}\times\left[\frac{e_{klij}(t)-e_{k+0.5}(t)}{(n+0.5)^2-(k+0.5)^2-(i+0.5)^2-(j+0.5)^2}-\frac{e_{kl}(t)-e_{k+0.5}(t)}{(n+0.5)^2-(k+0.5)^2-(l+0.5)^2}\right](i+0.5),$$

$$\alpha_4=0 \text{ for } \gamma<3$$

and

$$\alpha_4=\frac{3N_2}{\pi^7}\sum_{n=0}^{\infty}(n+0.5)^3\times s_{n+0.5}(x,t)\sum_{i=0}^{\infty}\frac{1}{i+0.5}\sum_{j=0}^{\infty}\left[\frac{1}{(n+0.5)^2-(i-j)^2}-\frac{1}{(n+0.5)^2-(i+j+1)^2}\right](j+0.5)^2\sum_{k=0}^{\infty}\frac{1}{k+0.5}\times\sum_{l=0}^{\infty}\frac{1}{l+0.5}\sum_{m_1=0}^{\infty}\frac{1}{m_1+0.5}\sum_{m_2=0}^{\infty}\frac{1}{m_2+0.5}\{[(j+0.5)^2-(k-l+m_1-m_2)^2]^{-1}+[(j+0.5)^2-(k-l-m_1+m_2)^2]^{-1}-[(j+0.5)^2-(k-l+m_1+m_2)^2)^2]^{-1}-[(j+0.5)^2-(k-l-m_1-m_2-1)^2]^{-1}-[(j+0.5)^2-(k+l+m_1-m_2-1)^2]^{-1}-[(j+0.5)^2-(k+l-m_1+m_2-1)^2]^{-1}+[(j+0.5)^2-(k+l-m_1-m_2)^2]^{-1}-[(j+0.5)-(k+l+m_1+m_2+2)^2]^{-1}\}\times\{[e_{iklm_1m_2}(t)-e_{n+0.5}(t)]\times[(n+0.5)^2-(i+0.5)^2-(j+0.5)^2-(k+0.5)^2-(l+0.5)^2-(m_1+0.5)^2-(m_2+0.5)^2]^{-1}[e_{ij}(t)-e_{n+0.5}(t)][(n+0.5)^2-(i+0.5)^2-(j+0.5)^2]^{-1}\}+\frac{4N_2}{\pi^7}\sum_{i=0}^{\infty}(i+0.5)^2s_{i+0.5}(x,t)\times\sum_{j=0}^{\infty}\sum_{l=0}^{\infty}\frac{1}{l+0.5}\times\sum_{l=0}^{\infty}\frac{1}{l+0.5}\sum_{n_1=0}^{\infty}\frac{1}{n_1+0.5}\sum_{n_2=0}^{\infty}(n_2+0.5)^2\{[(i+0.5)^2-(j-l-n_1+n_2)^2]^{-1}+[(i+0.5)^2-(j-l+n_1-n_2)^2]^{-1}-[(i+0.5)^2-(j+l+n_1-n_2+1)^2]^{-1}-[(i+0.5)^2-(j+l-n_1+n_1+1)^2]^{-1}-[(i$$

$+ 0.5)^2 - (j - k - n_1 + n_2 + 1)^2]^{-1} - [(i + 0.5)^2 - (j - l - n_1 - n_2 - 1)^2]^{-1} + [(i + 0.5)^2 - (j + l - n_1 - n_2)^2]^{-1} + [(i + 0.5)^2 - (j + l + n_1 + n_2 + 2)^2]^{-1}\} \sum_{k=0}^{\infty} \frac{1}{k + 0.5} \sum_{m=0}^{\infty} \{[(m + 0.5) - (n_5 - k)^2]^{-1} - [(m + 0.5)^2 - (n_2 + k + 1)^2]^{-1}\} \times((n_2 + 0.5)^2 - (k + 0.5)^2 - (m + 0.5)^2)^{-1}\{[e_{ijln_1km}(t) - e_{i+0.5}(t)][(i + 0.5)^2 - (j + 0.5)^2 - (l + 0.5)^2 - (n_1 + 0.5)^2 - (k + 0.5)^2 - (m + 0.5)^2]^{-1} - [e_{n_2}(t) - e_{i+0.5}(t)][(i + 0.5)^2 - (n_2 + 0.5)^2]\}$ for $\gamma = 3$,

$$C_{11}(x,t) = \alpha_5 + 2\alpha_6 + 2\alpha_7 - 2\alpha_8 + 2\alpha_9 + \alpha_{10} + 4\alpha_{11}, \qquad \text{(A5)}$$

where

$$\alpha_5 = \frac{\gamma D_1 N_2}{\pi^3} \sum_{l=0}^{\infty} s_{n+0.5}(x,t) \sum_{n=0}^{\infty} (n + 0.5)^3 \times \sum_{k=0}^{\infty} \frac{1}{k + 0.5} \sum_{m=0}^{\infty} \{[(m + 0.5)^2 - (n - k)^2]^{-1} - [(m + 0.5)^2 - (n + k + 1)^2]^{-1}\}((n + 0.5)^2 - (k + 0.5)^2 - (m + 0.5)^2)^{-1} \int_0^t [e_{km}(u) - e_{n+0.5}(u)] e_{l+0.5}(- u)[H_{l-n}(u) - H_{l+n+1}(u)]du,$$

$$\alpha_6 = \frac{\gamma D_1^2 N_2 L}{\pi^4} \sum_{n=0}^{\infty} (n + 0.5) s_{n+0.5}(x,t) \sum_{k=0}^{\infty} (k + 0.5)^3 \times \sum_{l=0}^{\infty} (l + 0.5)^2 \{[(l + 0.5)^2 - (n - k)^2]^{-1} - [(l + 0.5)^2 - (n + k + 1)^2]^{-1}\} \sum_{m=0}^{\infty} \int_0^t \frac{e_{kl}(u)}{e_{n+0.5}(u)} \int_0^u \tilde{e}_{ml}(\tau)[H_{l-m} + H_{l+m+1}]d\tau du,$$

$$\alpha_7 = \frac{D_1 N_2}{2\pi} \sum_{n=0}^{\infty} s_{n+0.5}(x,t) \sum_{m=0}^{\infty} \int_0^t [H_{m+n+1}(u) + H_{m-n}]\tilde{e}_{mn}(u)du,$$

$$\alpha_8 = \frac{\gamma D_1 N_2}{2\pi} \sum_{n=0}^{\infty} s_{n+0.5}(x,t) \times \sum_{m=0}^{\infty} \sum_{k=0}^{\infty} \frac{1}{k + 0.5} \int_0^t \frac{e_{km}(u)}{e_{n+0.5}(u)} [H_{n+k-m+0.5}(u) + H_{n-k+m+0.5}(u) - H_{n-k-m-0.5}(u) - H_{n+k+m+1.5}(u)]du,$$

$$\alpha_9 = 0 \text{ for } \gamma = 1,$$

$$\alpha_9 = \frac{\gamma D_1 N_2}{2\pi^3} \sum_{n=0}^{\infty} s_{n+0.5}(x,t) \sum_{k=0}^{\infty} \frac{1}{k + 0.5} \times \sum_{l=0}^{\infty} \frac{1}{1 + 0.5} \sum_{m=0}^{\infty} \int_0^t \frac{e_{klm}(u)}{e_{n+0.5}(u)} [I_{k-l-n+m}(u) + I_{k-l+n-m}(u) + I_{k-l-n-m-1}(u) + I_{k-l+n+m+1}(u) - I_{m-k-l+n}(u) - I_{k-l-n-m-1}(u) - I_{k+l+n-m+1}(u) - I_{m+k+l+n+2}(u)]du, \quad \text{for } \gamma \geq 2,$$

$$I_n = \int_0^L \eta(y,t)\cos(v_n y)dy,$$

$$\alpha_{10} = 0 \text{ for } \gamma < 3,$$

$$\alpha_{10} = D_1 N_2 \pi^{-5} \sum_{i=0}^{\infty} s_{i+0.5}(x,t) \sum_{n=0}^{\infty} (n + 0.5)^2 \int_0^t [I_{i-n}(u) + I_{i+n+1}(u)] \sum_{k=0}^{\infty} \frac{1}{k + 0.5} \sum_{l=0}^{\infty} \frac{1}{l + 0.5} \{[(i + 0.5)^2 - (j - k + l - n)^2]^{-1} + [(i + 0.5)^2 - (j - k - l + n)^2]^{-1} - [(i + 0.5)^2 - (j + k - l + n + 1)^2]^{-1} - [(i + 0.5)^2 - [(j + k - l - n + 1)^2]^{-1} - (i + 0.5)^2 - (j - k - l + n + 1)^2]^{-1} - [(i + 0.5)^2 - (j - k + l + n + 1)^2]^{-1} + [(i + 0.5)^2 - (j + k - l - n - 1)^2]^{-1} - [(i + 0.5)^2 - (j + k + l + n + 2)^2]^{-1}\} \sum_{m=0}^{\infty} \int_0^u \tilde{e}_{mn}(\tau)[I_{n-m}(\tau) + I_{n+m+1}(\tau)]d\tau du$$

for $\gamma = 3$,

$$\alpha_{11} = 0 \text{ for } \gamma \leq 2,$$

and

$$\alpha_{11} = \frac{D_1^2 N_2 L^3}{4\pi^6} \sum_{n=0}^{\infty} s_{n+0.5}(x,t) \sum_{k=0}^{\infty} \frac{1}{k + 0.5} \times \sum_{l=0}^{\infty} \frac{1}{l + 0.5} \sum_{m=0}^{\infty} \frac{1}{m + 0.5} \sum_{i=0}^{\infty} \int_0^t \frac{e_{klmi}(u)}{e_{n+0.5}(u)} \times [H_{k-n+i-l+m+0.5}(u) + H_{k-n-i+l-m+0.5}(u) + H_{k-n+l+i-m+0.5}(u) + H_{k+n-i-l+m+0.5}(u) - H_{k+n-i-l+m-0.5}(u) - H_{k-n+i+l-m+1.5}(u) - H_{k-n+i-l+m-0.5}(u) - H_{k+n-i+l-m+1.5}(u) + H_{k+n+i-l+m+1.5}(u) + H_{k-n-i+l-m-0.5}(u) + H_{k-n-i-l+m-0.5}(u) + H_{k+n+i+l-m+1.5}(u) - H_{k+n+i-l-m+0.5}(u) - H_{k-n-i+l+m+0.5}(u) - H_{k-n-i-l-m-1.5}(u) - H_{k+n+i+l+m+2.5}(u)]du \text{ for } \gamma = 3.$$

*Electronic address: elp@ipm.sci-nnov.ru

[1] V. G. Gusev and Yu. M. Gusev, *Electronics* (Vysshaya Shmkola, Moscow, 1991), in Russian.
[2] A. B. Grebene, *Bipolar and MOS Analogous Integrated Circuit Design* (Wiley, New York, 1983).
[3] T. Oka, K. Hirata, H. Suzuki, K. Ouchi, H. Uchiyama, T. Taniguchi, K. Mochizuki, and T. Nakamura, Int. J. High Speed Electron. Syst. **11**, 115 (2001).
[4] Z. Yu. Gotra, *Technology of Microelectronic Devices* (Radio i Syvaz', Moscow, 1991), in Russian.
[5] S. T. Sisianu, T. S. Sisianu, and S. K. Railean, Semiconductors **36**, 581 (2002).
[6] A. V. Chernyaev, Microelectronics **32**, 26 (2003).
[7] G. Masse and K. Djessas, J. Appl. Phys. **94**, 6985 (2003).
[8] R. N. Ghoshtagore, Phys. Rev. B **3**, 389 (1971).
[9] T. Ahlgren, J. Likonen, J. Slotte, J. Raisanen, M. Rajatora, and J. Keinonen, Phys. Rev. B **56**, 4597 (1997).
[10] O. V. Aleksandrov, Semiconductors **38**, 258 (2004).
[11] E. L. Pankratov, J. Mol. Liq. **114**, 179 (2004).
[12] E. L. Pankratov, Appl. Nonlinear Dyn. **12**, 35 (2004).
[13] Y. Y. Shan, P. Asoka-Kumar, K. G. Lynn, S. Fung, and C. D. Beling, Phys. Rev. B **54**, 1982 (1996).
[14] E. L. Pankratov, Tech. Phys. **74**, 115 (2004).
[15] T. I. Voronina, T. S. Lagunova, S. S. Kizhaev, S. S. Molchanov, B. V. Pushnyi, and Yu. P. Yakovlev, Semiconductors **38**, 556 (2004).
[16] E. Suvar, J. Christensen, A. Kuznetsov, and H. H. Radamson, Mater. Sci. Eng., B **102**, 53 (2003).
[17] A. N. Malakhov and E. L. Pankratov, Radiophys. Quantum Electron. **44**, 339 (2001).
[18] A. N. Malakhov and A. L. Pankratov, Adv. Chem. Phys. **121**, 356 (2002).
[19] W. T. Coffey, Yu. P. Kalmykov, and J. T. Waldron, *The Langevin Equation* (World Scientific, Singapore, 1996).
[20] W. T. Coffey, D. S. F. Crothers, and Yu. P. Kalmykov, Phys. Rev. E **55**, 4812 (1997).